



5-ALA localises to the autophagy compartment and increases its fluorescence upon autophagy enhancement through caloric restriction and spermidine treatment in human glioblastoma

Kim Fredericks^a, Jurgen Kriel^b, Lize Engelbrecht^b, Petra Andreea Mercea^c, Georg Widhalm^c, Brad Harrington^d, Ian Vlok^d, Ben Loos^{a,*}

^a Department of Physiological Sciences, Stellenbosch University, Stellenbosch, South Africa

^b Central Analytical Facility, Microscopy Unit, Stellenbosch University, South Africa

^c Department of Neurosurgery, Medical University of Vienna, Vienna, Austria

^d Department of Neurosurgery, Stellenbosch University, Cape Town, South Africa

ARTICLE INFO

Keywords:

Glioblastoma
5-Aminolevulinic acid fluorescence
Autophagy
Autophagosomes
Autolysosomes
Lysosomes
Autophagic activity

ABSTRACT

Glioblastoma Multiforme (GBM) is the most invasive and prevalent Central Nervous System (CNS) malignancy. It is characterised by diffuse infiltrative growth and metabolic dysregulation that impairs the extent of surgical resection (EoR), contributing to its poor prognosis. 5-Aminolevulinic acid (5-ALA) fluorescence-guided surgical resection (FGR) takes advantage of the preferential generation of 5-ALA-derived fluorescence signal in glioma cells, thereby improving visualisation and enhancing the EoR. However, despite 5-ALA FGR is a widely used technique in the surgical management of malignant gliomas, the infiltrative tumour margins usually show only vague or no visible fluorescence and thus a significant amount of residual tumour tissue may hence remain in the resection cavity, subsequently driving tumour recurrence. To investigate the molecular mechanisms that govern the preferential accumulation of 5-ALA in glioma cells, we investigated the precise subcellular localisation of 5-ALA signal using Correlative Light and Electron Microscopy (CLEM) and colocalisation analyses in U118MG glioma cells. Our results revealed strong 5-ALA signal localisation in the autophagy compartment – specifically autolysosomes and lysosomes. Flow cytometry was employed to investigate whether autophagy enhancement through spermidine treatment (SPD) or nutrient deprivation/caloric restriction (CR) would enhance 5-ALA fluorescence signal generation. Indeed, SPD, CR and a combination of SPD/CR treatment significantly increased 5-ALA signal intensity, with a most robust increase in signal intensity observed in the combination treatment of SPD/CR. When using 3-D glioma spheroids to assess the effect of 5-ALA on cellular ultrastructure, we demonstrate that 5-ALA exposure leads to cytoplasmic disruption, vacuolarisation and large-scale mitophagy induction. These findings not only suggest a critical role for the autophagy compartment in 5-ALA engagement and signal generation but also point towards a novel and practically feasible approach to enhance 5-ALA fluorescence signal intensity. The findings may highlight that indeed autophagy control may serve as a promising avenue to promote an improved resection and GBM prognosis.

1. Introduction

Glioblastoma, a grade IV brain tumour, is one of the most devastating cancers in humans, with an average patient survival time of 15 months post-diagnosis [1]. Treatment at diagnosis consists of maximum safe resection whenever possible, whereby the extent of resection (EoR) is a major prognostic factor. However, the characteristic infiltrative and

diffuse nature and metabolic dysregulation impairs the extent of successful surgical resection and negatively impacts tumour recurrence [2, 3]. Due to the frequently deep intracerebral localisation of these neoplasms and/or proximity to eloquent brain structures, the EoR is often compromised for the sake of preserving viable and functional neuronal tissue, so as to prevent neurological damage, thereby further-shortening the recurrence-free time [4]. The increased incidence of GBM, in

* Corresponding author. Department of Physiological Sciences, Merriman Avenue, Mike de Vries Building, Stellenbosch University, Stellenbosch, 7600, South Africa.

E-mail address: bloos@sun.ac.za (B. Loos).

<https://doi.org/10.1016/j.bbrep.2024.101642>

Received 20 October 2023; Received in revised form 29 December 2023; Accepted 8 January 2024

2405-5808/© 2024 Published by Elsevier B.V. This is an open access article under the CC BY-NC-ND license (<http://creativecommons.org/licenses/by-nc-nd/4.0/>).

conjunction with its aggressive nature and poor treatment outcome has led to the development of techniques and approaches aimed at increasing the EoR; one of which is based on 5-Aminolevulinic acid fluorescence-guided surgical resection (5-ALA FGR) representing one of the major advancements in neurosurgery in the last decades [5]. Metabolically, 5 ALA feeds directly into the haem biosynthetic pathway, and leads to the preferential accumulation of protoporphyrin IX (PpIX) within malignant cells – particularly those of higher grade, the reasons for which are poorly understood. The preferential accumulation paired with declining blood-brain barrier integrity, facilitates glioma-specific PpIX accumulation, and improved clinical outcomes have led to increased implementation of 5-ALA FGR in the management of gliomas. Indeed, 5-ALA FGR has now become the standard of care in the surgical management of patients suffering from GBM, particularly in Europe and the United States of America [6–8].

However, although 5-ALA FGR belongs to the widely-implemented surgical techniques in GBM resection, the associated fluorescent signal does not consistently allow for a clear identification of the tumour and its infiltrating margin. This is often caused by heterogeneity of the tumour itself, with recurrent tumours frequently emitting only weak fluorescence signal [9]. Furthermore, 5-ALA-derived fluorescence intensity has been shown to be poorest in the outermost, peripheral regions of GBM tumours *in situ* [10]. In this sense, infiltrative tumour tissue is still present in the tumour periphery in approximately half of cases despite the complete removal of all visible fluorescence (Kiesel et al. Journal of Neurosurgery; 2018). It is therefore critical to develop strategies to understand the subcellular organelles engaged with 5-ALA signal and to possibly enhance fluorescence intensity, so as to delineate the tumour margin more clearly, particularly in its infiltrative regions. In doing so, an enhanced visualisation of tumour borders would facilitate an improved EoR and consequently improved recurrence-free time.

Molecularly, a clear link between 5-ALA fluorescence and the mitochondrial network exists. Studies have shown a role for an increased abundance of mitochondria in increasing PpIX synthesis following 5-ALA administration [6]. The major metabolic dysfunction exhibited in GBM brings about a specific role for autophagy in cancer development and progression. Autophagy, the process by which long-lived and dysfunctional proteins are degraded in response to nutrient depletion or cellular stress, plays a dichotomous role in cancer [11]. Depending on the stage of tumour growth and progression, autophagy may confer cancer cell survival by providing metabolites to support high energy demands or suppress tumour progression by promoting gene stability and removal of degradative products [12–15]. However, despite the well-established interplay between the autophagy pathway and the mitochondrial cellular machinery, the relationship between the autophagy compartment and 5-ALA-derived fluorescence signal has not yet been investigated. In fact, the precise subcellular localisation of 5-ALA-derived fluorescence signal in GBM cells remains poorly understood, although evidence suggests a role of mitochondria, regions of exocytosis and even the plasma membrane [4,16–18]. This study therefore aimed to firstly characterise the localisation of 5-ALA-derived PpIX in malignant glioma cells at the subcellular level, including the cell's ultrastructural context, employing 3-dimensional (3-D) quantitative fluorescence and colocalisation analyses as well as correlative light and electron microscopy (CLEM) approaches. To improve clinical translational value, 5-ALA signal distribution was assessed in a 3-D spheroid model system, unravelling the relationship between autophagy flux and 5-ALA signal intensity across the glioma sphere. Finally, this study aimed to investigate the impact of autophagy enhancement on the magnitude of 5-ALA fluorescence signal generation, using the autophagy enhancing drug spermidine as well as nutrient deprivation. This study may implicate that 5-ALA-derived signal enhancement through autophagy induction, as employed in this study, may serve as a point of departure for clinical implementation to foster improved EoR and subsequent treatment outcome of GBM.

2. Materials and methods

2.1. Cell culture

U118MG cells were acquired from the American Type Culture Collection (ATCC, HTB-15™) and cultured using Dulbecco's Modified Eagle's Medium (DMEM) supplemented with 1 % Penicillin/Streptomycin (Pen Strep) (Life Technologies, 41 965 039 and 15 140 163) and 10 % Foetal Bovine Serum (FBS) (Capricorn Scientific, FBS-GI-HI-12 A) and incubated in a humidified incubator (SL SHEL LAB CO₂ Humidified Incubator) at 37 °C in the presence of 5 % CO₂.

In order to more accurately model the *in vivo* cell interactions and respective cell physiology that typically exists within a tumour micro-environment, 3-D spheroids were employed and generated using the hanging drop culturing technique adapted from Ref. [19]. In brief, 20 µL of filtered complete culture medium containing 2×10^4 cells was pipetted onto an inverted 90 mm³ Petri dish lid which was subsequently suspended over 16 mL phosphate buffered saline (PBS). Spheroids were grown for a minimum of 7 days before treatment intervention.

2.2. Reagents and transfection

5-Aminolevulinic Acid and Spermidine (SPD) were purchased from Sigma Aldrich (A3785 and S0266). Caloric restriction mimetic, Earle's Balanced Salt Solution was purchased from Life Technologies (14 155–048). Concentration and duration of exposure to SPD and CR was guided by previous work where robust autophagy enhancement was achieved [20,21]. 5-ALA was treated as light-sensitive and prepared in pre-chilled PBS. Bafilomycin A1 was purchased from LKT laboratories (B0025). GFP-LC3 (Addgene #21073 and GFP-LC3-RFP-LC3ΔG (Addgene # 84 572) plasmids were purchased from Addgene. For clonal expansion, bacteria were plated on agar plates using pre-mixed LB broth with Agar (Sigma, L3147) in the presence of Ampicillin (Roche, Cat # 10 835 242 001) and incubated overnight at 37 °C. Thereafter, inoculation of selected colonies was performed by pipetting bacteria into 5 mL pre-mixed LB broth (Sigma, L3522) and incubating overnight at 37 °C in a shaking incubator. Thereafter, 100 mL of fresh LB broth was inoculated with 1 mL of overnight culture and placed back into the shaking incubator overnight at 37 °C. Lastly, plasmid purification was conducted using a QIAGEN Plasmid Midi Kit (Qiagen, 12 143) as per the manufacturer's instructions. Following plasmid purification, U- 118 MG cells were transfected using the X-tremeGENE HP Transfection Reagent (Sigma-Aldrich, 06 366 236 001). Transient transfection was achieved according to manufacturers' guidelines with a plasmid concentration of 165.7 ng/µL in a 3:1 ratio and cell density of 7.5×10^3 .

2.3. Confocal and correlative light and electron microscopy

U118MG cells were transiently transfected with GFP-LC3 and untransfected cells stained with 50 nM LysoTracker™ Red DND-99 and 75 nM MitoTracker® DeepRed FM, respectively. Cells were seeded at a density of 7.5×10^3 cells per 35 mm³ confocal dish and allowed to adhere overnight. Thereafter, transfected cells and those stained with LysoTracker, were treated with 5 mM 5-ALA for 6 h and fixed in 4 % paraformaldehyde (PFA) for 10 min at 37 °C. The monolayer was rinsed with PBS at room temperature and thereafter stored in PBS on ice until image acquisition was performed. PBS was aspirated before imaging and cells mounted in Dako fluorescence mounting media. 5-ALA-treated cells stained with MitoTracker® were imaged live using the top-stage incubator on the Carl Zeiss LSM 780 PS.1 confocal microscope, pre-heated to 37 °C. Untreated, control U118MG cells were transfected and counterstained with LysoTracker® Red and Hoechst 33 342. Cells were acquired using a 63× magnification oil immersion objective and Zen® 2012 software. A minimum of 18 cells were acquired per treatment group, with each z-stack including 10 image frames at a step width of 0.4 µm. Images were deconvolved using the EpiDEMIC plugin

available in Icy Bioimaging software (<http://icy.bioimageanalysis.org/plugin/epidemic/>) [22] and analysis was conducted using the ImageJ Colocalisation Threshold plugin. Pearson's correlation coefficients were interpreted as follows: $r = 0.9-1$, very strong correlation; $0.7-0.89$, strong correlation; $0.4-0.69$, moderate correlation; $0.1-0.39$, weak correlation, $0-0.09$, negligible correlation [23]. Manders' colocalisation coefficient represents the fraction of fluorescent signal from one channel that colocalises with structures on the other channel. Note, there is no Pearson's correlation coefficient for the colocalisation analysis between autolysosomes and 5-ALA signal, because the autolysosome channel was generated as a mask, hence only indicating absolute intensities. For this reason only the Mander's correlation coefficient could be generated as it is a reflection of co-occurrence of signal from two channels - that is the fraction of one signal that co-occurs with the other.

Autophagy flux analysis. Stably transfected GFP-LC3-II-RFP-LC3ΔG U118MG cells were cultured into 3-D spheroids for a minimum of 7 days, whereafter they were treated with 5 mM 5-ALA for 6 or 24 h and fixed using 4 % PFA for 30 min at 37 °C in 5 % CO₂. Spheroids were acquired as z-stacks using the Carl Zeiss LSM 780×confocal microscope and 10× magnification using the Zen® 2012 software. The ratio of GFP/RFP is indicative of autophagy flux, where a low ratio is indicative of a high autophagy flux and *vice versa* [24]. For the purposes of visualising the relative autophagy activity in relation to 5-ALA signal localisation, the ImageJ Image Calculator plugin was used to determine the ratio of RFP/GFP. Thereafter a lookup table (LUT) was applied to the ratiometric micrograph and autophagy flux 'hotspots' were represented on the LUT as areas where the signal ratio was highest. Next, ratiometric images were overlaid with the channel corresponding to 5-ALA-derived fluorescence to show the localisation of both signals. Transiently transfected GFP-LC3-II U118MG cells were seeded at a density of 7.5×10^4 cells in a 35 mm³ confocal dish and allowed to adhere overnight. Thereafter transfected cells were treated with 5 mM 5-ALA for 6 h and 400 nM Bafilomycin A1 for 4 h. Control, transiently transfected GFP-LC3 cells were only treated with 5 mM 5-ALA for 6 h. Live cells were acquired using the top-stage incubator on the Carl Zeiss LSM 780 PS.1 confocal microscope, pre-heated to 37 °C, a 63× magnification oil immersion objective and Zen® 2012 software. A minimum of 3 cells was acquired per treatment group, with each z-stack including 10 image frames with a step width of 0.8 μm. Maximum intensity projections were generated using ImageJ. Cells were delineated as ROIs and the average background fluorescence signal was quantified as the mean of 3 equal-sized ROIs acquired using the Image J Measure Plugin. Thereafter, corrected mean fluorescence intensity (MFI) values were generated as the difference of each cell's mean fluorescence intensity and average background fluorescence signal.

Correlative light and electron microscopy. U118MG cells were seeded at a density of 7.5×10^4 cells in a gridded coverslip dish (Mattek) and incubated overnight. To assess 5-ALA-derived fluorescence-positive puncta and autophagosomes, cells were transiently transfected with GFP-LC3. Cells were then treated with 5 mM 5-ALA for 6 h, following an addition of 50 nM LysoTracker® Red DND-99 in the last 30 min, control cells were not treated with 5-ALA. Thereafter, cells were fixed with 4 % PFA in at 37 °C and rinsed in PBS before being transferred to the Zeiss LSM 780 confocal microscope. A tile scan was performed at 10× magnification in order to identify the grid coordinates on the coverslip and to locate suitable regions of interest. The coordinates of each cell in the grid block of interest were set and annotated on the Zen® 2012 software to allow for later accurate identification and trimming of the resin block [25]. Each region of interest was acquired through a z-stack of approximately 15 micrographs at 63× magnification using a 405 nm, 488 nm and 561 nm laser excitation along with a transmission photomultiplier tube (TPMT) channel to assist in subsequent CLEM overlay. Each micrograph was acquired at a step width of 0.4 μm per image stack.

Electron microscopy sample preparation. After acquisition of the FM micrographs, cells were further fixed using 2.5 % glutaraldehyde and 4 % formaldehyde in 0.1 M Sorenson's phosphate buffer at room

temperature for 30 min. Cells were washed in dH₂O prior to incubation with the following solutions: 2 % reduced osmium tetroxide on ice for 1 h (made with 1:1 dilution of 4 % OsO₄ and 3 % potassium ferricyanide), Thiocarbohydrazide (TCH) at room temperature for 20 min, aqueous osmium tetroxide at room temperature for 30 min and an overnight incubation at 4 °C in 1 % uranyl acetate (Tapia et al., 2012). Each incubation was followed by wash steps using dH₂O. The next day, samples were washed using dH₂O and incubated in 0.03 M lead aspartate at room temperature for 30 min and rinsed dH₂O. Next, samples were dehydrated in a series dilution of EtOH (20 %, 50 %, 70 %, 90 %, 100 % and anhydrous 100 %), for 5 min each on ice. The final dehydration step with 100 % anhydrous EtOH was repeated at room temperature for 10 min. The samples were then incubated in a mixture of propylene oxide and Durcupan diluted 1:1 at room temperature for 1 h, followed by 2 additional 90-min incubation steps in 100 % Durcupan at room temperature. Lastly, a flat-bottom capsule (Agar Scientific Ltd, Essex, UK, G3759) was filled with fresh 100 % Durcupan and inverted onto the selective area previously marked with a permanent marker. This sample assembly was then incubated at 60 °C for at least 48 h to facilitate polymerisation. Next, the inverted capsule was detached from the coverslip, with cells now having been transferred to the Durcupan - and the resin block was then further sectioned using a Leica UC7 ultramicrotome system (Leica Microsystems, Austria) equipped with an Ultra 45° 3 mm diamond knife (Diatome US, Hatfield, PA, USA, MS16427). Sections of 100 nm thickness were cut and collected on 5 × 5 mm silicon wafer squares (Agar Scientific Ltd, Essex, UK, G3390). Silicon wafers were mounted onto 12 mm aluminium SEM specimen stubs using double-sided carbon conductive tape (AGG3935, Agar Scientific). The 10× magnification tile image acquired during the FM acquisition was used as a coordinate map and guided the initial visualisation of the cells on the silicon wafers using the ThermoFisher Apreo Volumescape FESEM (FEI, Netherlands). Cells of interest were acquired at various depths in the z-axis to facilitate a more accurate overlay at a later stage in the CLEM workflow. All micrographs were acquired at an accelerating voltage of 5 kV and a probe current of 1.6 nA using the T1 trinity detectors with immersion lens use-case in TIF format at a resolution of 3072×2034 pixels.

FM and EM micrograph overlays. Electron and fluorescence micrographs were overlaid using the EC-CLEM plugin in Icy Bioimaging software using a minimum of 25 landmark points of interest to generate an accurate overlay (<http://icy.bioimageanalysis.org/plugin/ec-CLEM/>) [26].

Serial block-face scanning electron microscopy (SBF-SEM). Spheroids were treated with 5 mM 5ALA for 6 h and thereafter fixed in 4 % paraformaldehyde for 30 min at room temperature. Spheroids were prepared according to the abovementioned EM preparation protocol. Following resin embedding, the resin block was trimmed to a ROI area of $0.5 \times 0.5 \times 1$ mm using a Leica UC7 ultramicrotome system (Leica Microsystems, Austria) equipped with a glass knife. Excess epoxy was trimmed off and fine cutting of the resin block continued with the ultramicrotome, using a diamond knife (Diatome, USA). The block-face was then sputter coated with 50 nm gold/palladium (Denton Desk V, USA) followed by another step of ultra-microtoming (100 nm thin sections) to only expose the sample block-face. The stub was placed into the ultra-microtome attachment of the Apreo Volumescape and eucentric calibration of the diamond knife to the block-face was conducted. After confirming alignment of the sample to the knife, the sample chamber was closed and pumped to the appropriate vacuum. Image acquisition was conducted at an adjusted chamber pressure of 0.5 mbar to compensate for excessive charging of the resin. Under low vacuum, the VolumeScope Dual Back Scatter (VS DBS) detector was implemented, using a voltage of 3.00 kV and probe current of 0.20 nA. Region finding and beam energy alignment was conducted using Xt Microscopy and Maps 3.9 software (ThermoScientific). A z-width of 50 nm was chosen as cutting thickness. Sample polishing commenced at 50 nm thickness for 100 slices to confirm a eucentric cutting angle. Thereafter, serial block-

face data was acquired for a total of 200 slices per sample using the VS-DBS detector at a pixel resolution of 3840×2160 with a scan speed of $2 \mu\text{s}$. Low electron density regions of each series of SBF images were rendered volumetrically.

Flow cytometry mean fluorescence intensity analysis. The mean fluorescence intensity of live U118MG cells was assessed through flow cytometry using the BD FACSMelody™ Cell Sorter (BD Biosciences). A total of 15 000 events was recorded for each treatment group, where 5-ALA fluorescence was detected at an excitation/emission 405/635 nm. Flow cytometry FCS files were analysed using FlowJo™ Software to enable gating on the cell population while excluding debris.

2.4. Statistical analysis

Statistical analysis was performed using GraphPad Prism 7.04 software for Windows. One-way ANOVA was performed and followed by Bonferroni's post-hoc test after normal distribution was confirmed using the Shapiro-Wilk test. A p value < 0.05 was considered significant. Results were presented as mean \pm standard error of the mean (SEM).

3. Results

While 5-ALA is widely established in the clinical setting to guide surgical resections of GBMs, very little information is known regarding the subcellular localisation of 5-ALA derived fluorescence and underlying molecular mechanisms. Consequently, this study undertook to establish the precise localisation of 5-ALA-derived fluorescence within the cell. To reveal the nature of the relationship between 5-ALA and the autophagy pathway intermediates, 5-ALA localisation to autophagosomes, autolysosomes and lysosomes was assessed using colocalisation analysis.

3.1. 5-ALA colocalisation analysis

The colocalisation between 5-ALA-derived fluorescence signal and GFP-LC3 signal was comparatively weakest amongst the three organellar structures assessed [0.18 ± 0.05] (Fig. 1), when using a Pearson's correlation coefficient. However, a large portion of 5-ALA-derived puncta co-occurred with autophagosomes with a M1 colocalisation coefficient of $0.773 [\pm 0.0199]$ (Fig. 1. A). Notably, autophagosomes displayed a low co-occurrence with 5-ALA-derived punctate structures with a M2 of $0.486 [\pm 0.0418]$. Although the colocalisation of 5-ALA-derived signal was not as high as that observed in lysosomes, the positive signal correlation taken together with the colocalisation metrics support the relation between 5-ALA-derived fluorescence and LC3-positive organelles (Fig. 1. B). Colocalisation of 5-ALA-derived signal with lysosomes revealed a strongly positive correlation between these two structures, with a Pearson's correlation coefficient of $0.73 [\pm 0.03]$ (Fig. 1. C). This strong correlation between 5-ALA derived signal and lysosomes was also visually supported with large 5-ALA positive structures colocalising strongly with large lysosomal structures (Fig. 1. D). Manders' colocalisation coefficient analysis confirmed that a large portion of 5-ALA derived-signal co-occurs with lysosomal structures [0.93 ± 0.01] and similarly, lysosomal signal largely co-occurs with 5-ALA-derived fluorescence [0.85 ± 0.02]. Taken together it is therefore evident that 5-ALA signal is largely lysosomal in nature.

Next, we assessed the colocalisation of 5-ALA derived signal with autolysosomes (Fig. 1. E, F). The subsequent colocalisation analysis showed that a large portion of 5-ALA signal co-occurred with autolysosomes [0.89 ± 0.02] while to a lesser extent co-occurrence of autolysosome signal with 5-ALA puncta [0.57 ± 0.06] was observed. This confirms the involvement of the autophagy pathway and suggests the existence of a pool of 5-ALA-negative autolysosomes. The biochemical mechanisms that inform 5-ALA-FGR indicate an integral role of mitochondria in the conversion of exogenous 5-ALA to the photosensitising PpIX; for this reason, we assessed the relationship between 5-ALA-

derived fluorescence and the mitochondrial network of the cell. Our results reveal the degree of correlation and colocalisation between 5-ALA-derived fluorescence and mitochondria, with a Pearson's correlation coefficient $r = 0.375 [\pm 0.07]$, indicating a weak positive correlation (Fig. 1. G). This correlation is, compared to the other organelles assessed, indicative of poor co-distribution of mitochondrial- and 5-ALA-derived signal. Notably, however, the Manders colocalisation coefficients were high in value, indicative of a high proportion of spatial overlap of 5-ALA-derived signal and that corresponding to mitochondria. In addition, the nature of 5-ALA-derived signal was similar to the punctate signal acquired during characterisation (Fig. S. 2. C, D), although here it appears slightly more diffusely dispersed throughout the cytoplasm of the cell (see Fig. 1. H).

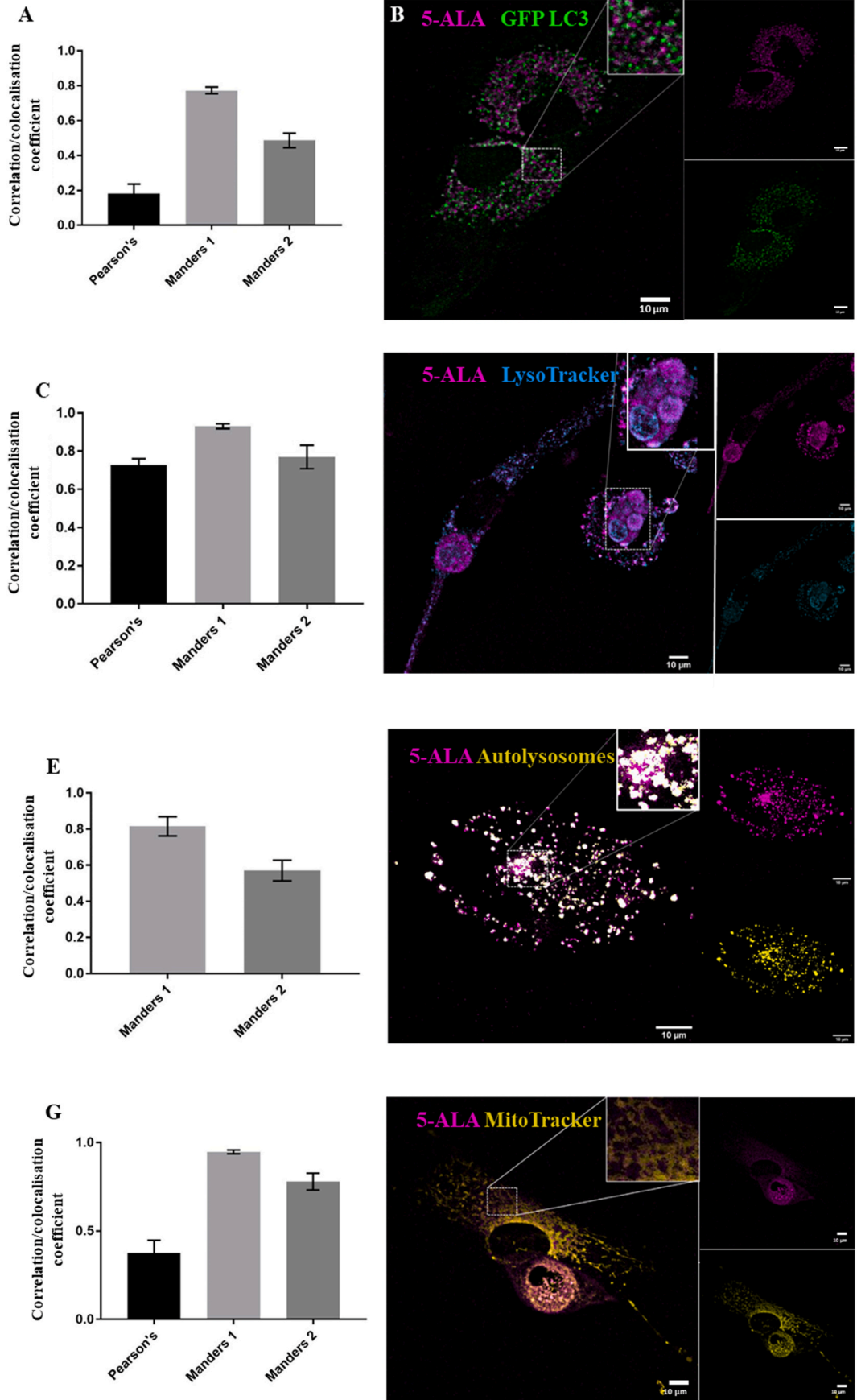
3.2. 5-ALA and autophagy flux

Next, a 3-D tumour spheroid model was employed to investigate the relationship between 5-ALA-derived fluorescence signal and autophagy flux, taking advantage of this clinically relevant model system stably expressing the GFP-LC3-II-RFP-LC3ΔG plasmid. Initial comparison of the GFP-LC3-II-RFP-LC3ΔG signal revealed an apparent increase in RFP LC3ΔG signal after 24 h of 5-ALA treatment compared to 6 h 5-ALA exposure (Fig. 2. B, C). Following ratiometric rendering, autophagy flux hotspots presented as areas where the ratiometric signal was highest, allowing to visually discern cells with high or low autophagy activity. Notably, an increased 5-ALA-derived fluorescence signal intensity in the central regions was observed, corresponding to cells with relatively high autophagy flux, with increased 5-ALA signal also in areas of the spheroid periphery. More of such overlapping signal hotspots were present upon 24-h 5-ALA treatment intervention (Fig. 2. C, E). Mean fluorescence intensity analysis and quantification revealed that spheroids treated with 5 mM 5-ALA for 24 h displayed the most drastic increase in autophagy flux, showing the lowest GFP/RFP ratio – albeit not reaching significance (Figs. S1A and B).

Correlative light and electron microscopy (CLEM) was employed to investigate the ultrastructural context of 5-ALA-derived fluorescence signal, given the results reported in the previous section. Our results reveal that 5-ALA exposure resulted in a disruption of the cytoplasmic environment, supported by the presence of large vacuolar structures occupying a major portion of the cytoplasm and overall scarcity of mitochondria. Autophagosomes were observed scattered predominantly in the peripheral regions of the cells, particularly when compared to the apparent abundance of lysosomes. Further qualitative comparison of the fluorescence signal corresponding to autophagosomes and lysosomes showed highly distinct size differences, specifically the larger lysosomes, upon 5-ALA exposure (Fig. 3 I, ii). Lysosomes showed a distinctively high electron density when compared to that of the cytoplasm (Fig. 3C I, ii, iii).

Initial assessment of cells treated with 5 mM 5-ALA revealed that distinct changes in cellular cytoplasmic arrangement and contents were induced (Fig. 4). Notably, a visible increase in the number of autophagosomes was apparent upon 5-ALA treatment when compared to control cells (Fig. 4 A, i). Further assessment of 5-ALA treated cells showed increased cytoplasmic disruption evident by the relative increase of large, vacuolar structures visible throughout the cytoplasm (Fig. 4 ii, iii). Furthermore, a clear relative increase in vacuoles scattered throughout the cell with no specific relation to the identity of autophagosomes, lysosomes or 5-ALA puncta was observed (Fig. 4 B).

Most importantly, and in agreement with the colocalisation analysis, large lysosomal structures showed a strong association with 5-ALA-derived fluorescence. Punctate structures positive for 5-ALA signal overlapped with lysosomes. Strongest 5-ALA fluorescence typically originated in punctate structures that overlapped with mainly signal from autolysosomes (Fig. 4C (i)) and to a lesser extent, autophagosomes (Fig. 4C). Electron micrographs shown depict electron-dense vesicles corresponding to 5-ALA-derived fluorescence containing clusters of



(caption on next page)

Fig. 1. A) Pearson's correlation coefficient r , Manders colocalisation coefficients 1&2 from GFP-LC3 transfected U118MG cells following 6-h 5 mM 5-ALA treatment, $N = 18-22$. B) Representative micrograph of U118MG cells indicating GFP-LC3 signal after 6-h 5 mM 5-ALA treatment. C) Pearson's correlation coefficient r , Manders colocalisation coefficients 1&2 from U118MG cells counterstained with LysoTracker® Red following 6-h 5 mM 5-ALA treatment, $N = 18-22$. D) Representative micrograph of U118MG cells indicating LysoTracker® Red counterstaining (painted cyan) after 6-h 5 mM 5-ALA treatment. E) Manders colocalisation coefficients 1&2 from U118MG cells indicating autolysosomes (mask rendered GFP-LC3 and LysoTracker® Red colocalisation, painted in yellow) after 6-h 5 mM 5-ALA treatment, $N = 18-22$. F) Representative micrograph of U118MG cells indicating mask representing autolysosomes after 6-h 5 mM 5-ALA exposure. G) Pearson's correlation coefficient r , Manders colocalisation coefficients 1&2 from U118MG cells counterstained with MitoTracker® DeepRed following 6-h 5 mM 5-ALA treatment, $N = 18-22$. H) Representative micrograph of U118MG cells indicating MitoTracker® DeepRed counterstaining (painted gold) after 6-h 5 mM 5-ALA treatment. Scale bar: 10 μm . (For interpretation of the references to colour in this figure legend, the reader is referred to the Web version of this article.)

material that appear membranous in nature (Fig. 4C (i)).

3.3. The effect of 5-ALA on cellular ultrastructure in GBM spheroids

Next, we further investigated the effect of 5-ALA exposure on U118MG spheroids in terms of ultrastructural arrangement and detail. Serial Block Face Scanning Electron Microscopy (SBF SEM) was performed, to visualize the entire sphere, revealing its core ultrastructure (Fig. 5 A, B). EM analysis revealed a loosely organised periphery in control spheres, while in 5-ALA exposed spheres, a dense, more highly packed cellular arrangement emerged, with a less apparent electron-dense periphery in comparison to the well-defined, electron-dense peripheral region in control spheres (Fig. 5 A, B). Long, interconnected segments of the mitochondrial network were observable in control spheroids, interspersed between spherical mitochondria with partially disrupted cristae (Fig. 5C). Intriguingly, spheroids treated with 5 mM 5-ALA for 6 h showed a distinct disruption of mitochondria and revealed substantial evidence for the induction of mitophagy (Fig. 5 D). In addition, mitochondria and double-membrane structures were rearranged in a highly convoluted fashion around strikingly rounded and shrunken mitochondria that appear to lack cristae (Fig. 5 D). It was further evident that 5-ALA treatment disrupted the overall cytoplasmic organisation of the cell.

To characterise the effects of 5-ALA treatment on the overall morphological integrity of 3-D spheroids, SBF-SEM was employed to acquire entire spheroids and reveal their ultrastructure in 3-D. Substantial abundance of structures low in electron density, likely massive vacuolar structures, were observed following volumetric rendering (Fig. 5 E, F). A robust effect of 5-ALA exposure on both size and abundance of these structures was observed, indicated by their increase in volume and number (Fig. 5 F). When comparing these vacuolar structures, it was noted that control spheres are characterised by small, widely dispersed structures throughout the core (Fig. 5 F), while, in sharp contrast, 5-ALA exposure resulted in an increased number of larger, vacuolar structures more densely arranged within the core.

Further interrogation of the cellular ultrastructure of control U118MG spheroids using high resolution SBF-SEM showed a distinct status of the mitochondrial network in cells that form part of the outer proliferative layer (Fig. S3 A). Here we observed round mitochondria with disrupted cristae as well as elongated mitochondrial structures in and amongst an electron dense, highly disrupted cytoplasm. Furthermore, an indication for a necrotic core was provided due to the presence of lucent cytoplasm, cytoplasmic and organelle swelling and nuclear degeneration (Fig. S3 B). In contrast, further investigation of the ultrastructure of the mitochondrial network following 5-ALA treatment revealed a highly disrupted mitochondrial network comprised of primarily round mitochondria with indistinguishable cristae (Fig. S3 C, D). In addition to mitochondrial disruption, large, vacuolar structures low in electron density were observed towards the core of 5-ALA treated spheroids (Fig. S3 D). Additionally, several cells showed evidence for necrosis – comparatively more than were observed in untreated spheroids (Fig. S3 D).

3.4. 5-ALA fluorescence and autophagy induction

To assess the effects of autophagy in 5-ALA signal intensity, two

means of autophagy induction, namely caloric restriction and spermidine exposure, were employed. 5 mM 5-ALA in combination with SPD caused an increase in 5-ALA fluorescence intensity [$104.68 \pm 1.22\%$ ($p < 0.05$)] relative to cells treated with 5 mM 5-ALA only; where CR [$109.29 \pm 1.33\%$ ($p < 0.05$)] and the combination of CR and SPD [$125.47 \pm 1.33\%$ ($p < 0.05$)] treatment showed a much greater increase in 5-ALA mean fluorescence intensity with the combination treatment showing the most robust increase. Relative to 5-ALA and SPD treated cells, treatment groups subjected to CR and the combination of SPD and CR ($p < 0.05$) significantly increased 5-ALA-derived fluorescence intensity ($p < 0.05$), with SPD and CR combination treatment further increasing fluorescence intensity relative to 5-ALA and CR co-treatments ($p < 0.05$) (Fig. 6 A, B). Indeed, SPD exposure showed the lowest relative increase in mean fluorescence intensity compared to 5-ALA-only treated cells, whilst cells treated with 5-ALA and CR presented with a relatively greater increase in fluorescence intensity while the combination of 5-ALA, CR and SPD treatment caused the highest increase in 5-ALA-derived fluorescent signal intensity. Finally, bafilomycin A1 (Baf) inhibits the fusion of autophagosomes and lysosomes, increased accumulation of LC3-II-positive structures is therefore indicative of increased autophagy flux. Transiently transfected GFP-LC3 cells treated with 5-ALA and those treated with Baf were imaged to represent the effect of 5-ALA on this pathway (Fig. 6 G, H).

4. Discussion

4.1. 5-ALA localises primarily to the autophagy compartment

Currently, little consensus exists regarding the subcellular localisation of 5-ALA. Some studies have relied on the biochemical pathway analysis and pointed to its mitochondrial localisation, whilst others indicated exocytosis of 5-ALA after its synthesis [4,17]. Also the plasma membrane has been suggested with a general cytosolic distribution of 5-ALA signal [16,18]. Consensus however exists that the localisation of 5-ALA derived PpIX is largely dependent on cell type and differs depending on the disease state [16,18]. Our results revealed specific and predominant localisation of 5-ALA to the LC3 positive compartment in glioma cells, which had not previously been shown and led us to further dissect whether 5-ALA fluorescence was specific to mitochondria and autophagy pathway intermediates, i.e. lysosomes, autophagosomes or autolysosomes. Colocalisation analysis along with CLEM analysis revealed specifically the localisation of 5-ALA primarily to lysosomes (Fig. 1C, D). Furthermore, we demonstrate the localisation of 5-ALA, albeit to a lesser extent, with the autophagy pathway intermediates – autophagosomes and autolysosomes (Fig. 1 A, B, E, F). Our quantitative analysis of localisation through Pearson's and Manders correlation and colocalisation coefficients, illustrated the correlation and co-occurrence of signal on either channel. This enabled a great degree of precision, revealing the localisation of 5-ALA preferentially to lysosomes in U118MG cells. Moreover, a significant colocalisation of 5-ALA with autolysosomes was revealed in this manner, further supporting the involvement of autophagy in subcellular 5-ALA derived signal localisation (Fig. 1 E, F). It remains evident that a relationship indeed exists between 5-ALA-positive punctate structures and autolysosomes due to their high spatial colocalisation (Fig. 1 E, F). It was further shown that 5-ALA correlated with autophagosomes to a lesser extent in U118MG

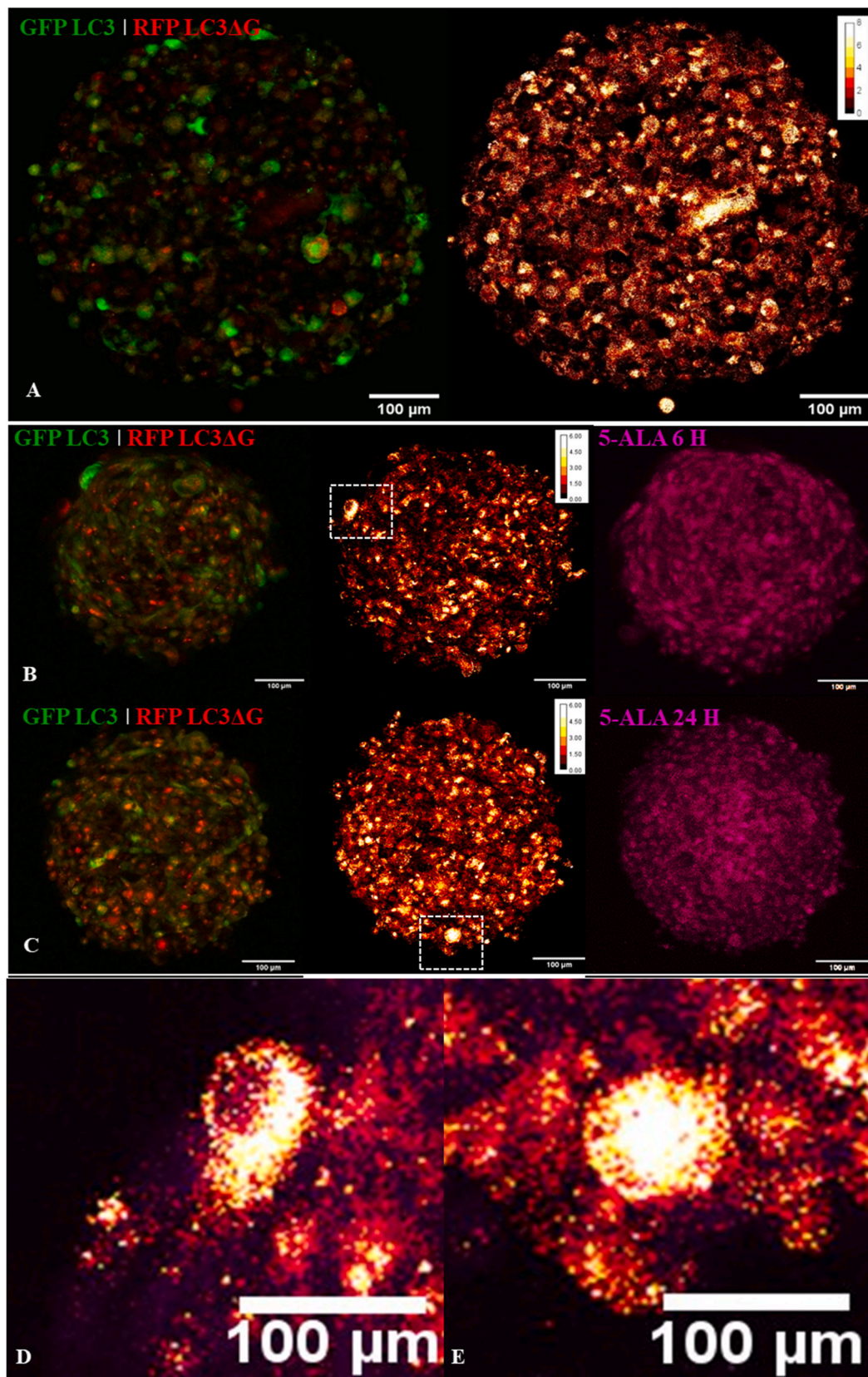


Fig. 2. A) U118MG cells stably transfected with the GFP-LC3-II-RFP-LC3ΔG plasmid indicating autophagy flux were used to generate 3-D spheroids with corresponding ratiometric render (pictured right) depicting the ratio of GFP/RFP fluorescence signal. B) Autophagy flux upon 6 h 5 mM 5-ALA exposure with areas of high autophagy flux corresponding to regions with high 5-ALA-derived fluorescence signal indicated with white boxes. Ratiometric render (pictured right) shows regions of high autophagy flux and corresponding 5-ALA-derived signal. C) Autophagy flux upon 24 h 5 mM 5-ALA exposure with areas of high autophagy flux corresponding to regions with high 5-ALA-derived fluorescence signal indicated with white boxes. D, E) Regions of interest show high 5-ALA signal corresponding to areas of heightened autophagy flux. Scale bar: 100 μm .

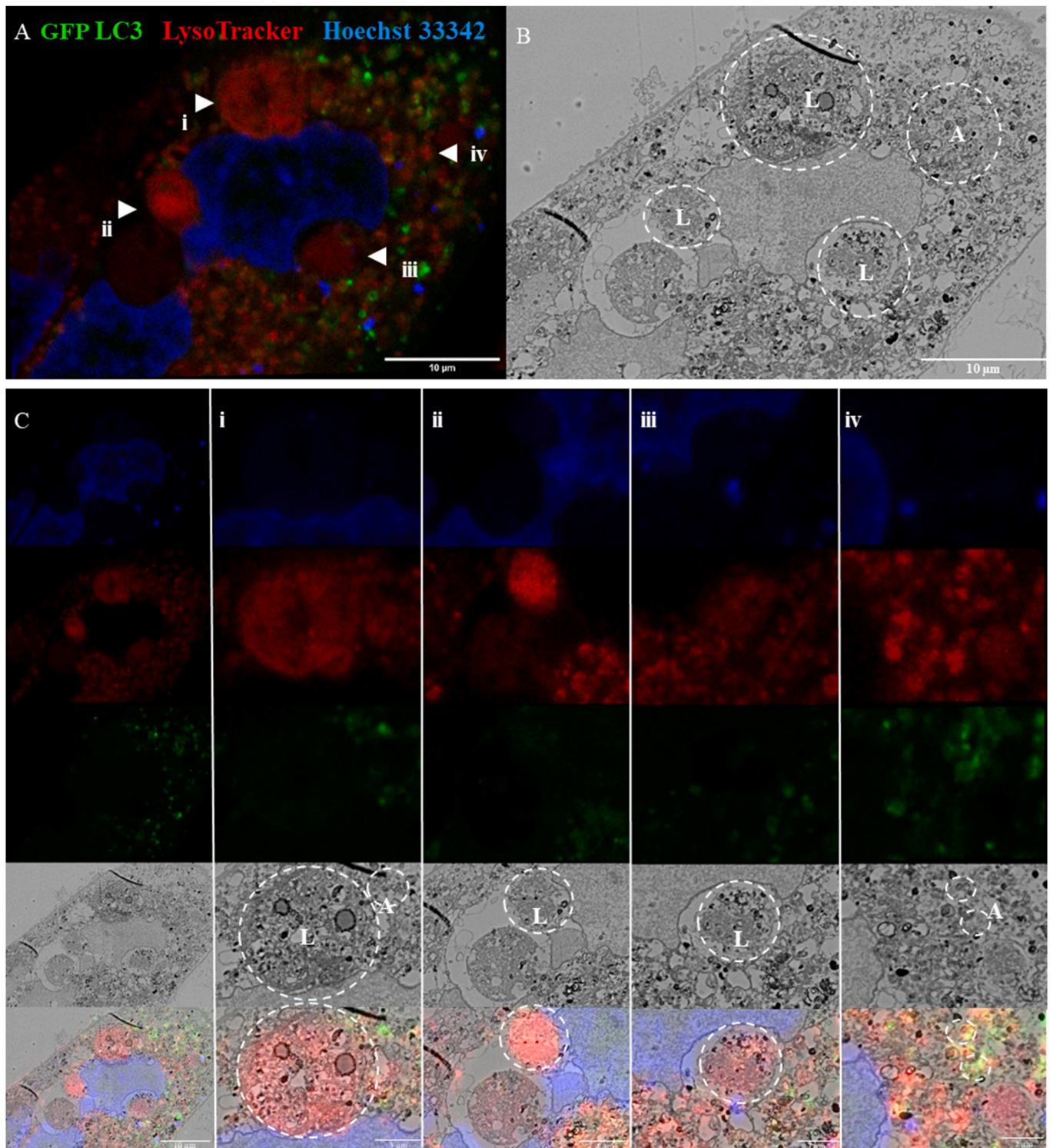
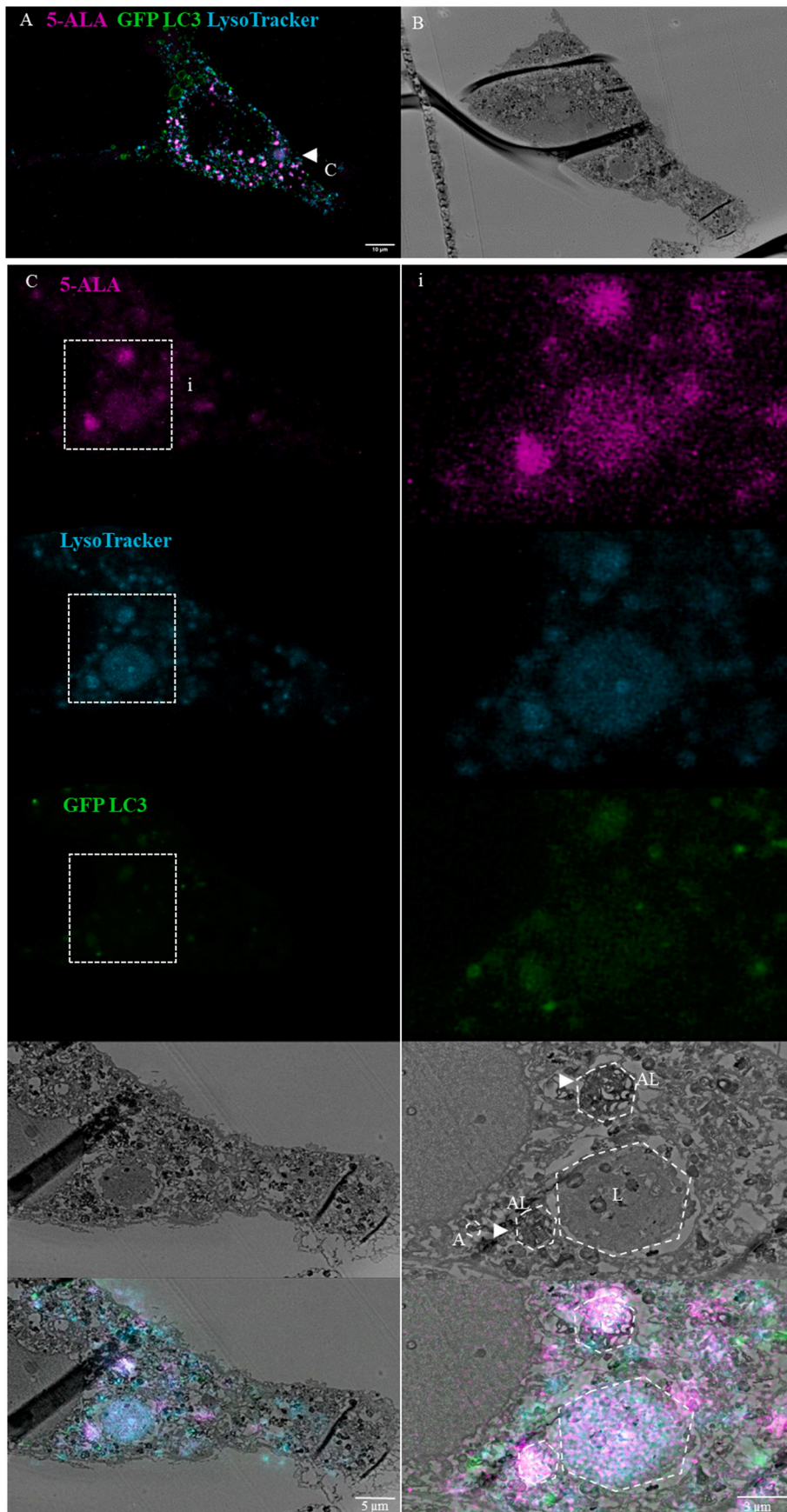


Fig. 3. Fluorescence microscopy (FM) and electron microscopy (EM) micrographs depicting representative 5-ALA untreated U118MG cell. (A, B) Representative FM and EM image showing overview and regions of interest i.e., lysosomes and autophagosomes indicated with white arrowheads, labelled i, ii, iii, iv. C (i, ii, iii, iv) CLEM images, FM and EM micrographs showing overview region of representative 5-ALA untreated cell, counterstained with Hoechst 33 342, and zoomed-in regions of interest highlighted in (i, ii, iii, iv). A (Autophagosomes), L (Lysosomes). FM images acquired using 63 \times magnification, scale bars: (A, B, C) 10 μ m; (i, ii) 3 μ m, (iii) 4 μ m, (iv) 2 μ m.

cells, despite the high degree of colocalisation with GFP-LC3-positive puncta (Fig. 1 (A, B)), suggesting the presence of a 5-ALA-negative autophagosome pool. Indeed, a recent study reported a similar pattern in 5-ALA signal localisation, supporting our findings of 5-ALA localisation to lysosomes. There, a panel of various cell types was employed

to investigate the correlation of 5-ALA with mitochondria, ER, Golgi and lysosomes [27]. Interestingly, Sasaki et al. [27] reported the highest amount of 5-ALA produced in MCF7 breast cancer and PC3 prostate cancer cells, supporting the notion of cell specific 5-ALA metabolism. Our results reveal a clear role specifically for the autophagy-lysosome



(caption on next page)

Fig. 4. Fluorescence and EM micrographs showing U118MG cell following 6-h 5 mM 5-ALA treatment exposure. (A, B) Representative FM and EM image showing overview and regions of interest, i.e., 5-ALA-positive autolysosomes, lysosomes and autophagosomes, indicated with white arrowheads and boxes, labelled C. C (i) CLEM images, FM and EM micrographs showing overview region of a representative 5-ALA treated cell and zoomed-in regions of interest highlighted in C, C (i). A (Autophagosomes), AL (Autolysosome), L (Lysosome). FM images acquired using 63 \times magnification, scale bars: (A, B) 10 μ m; (C) 5 μ m and (C (i)) 3 μ m.

pathway for 5-ALA derived fluorescence signal generation. In contrast, a much lower portion of 5-ALA signal associated with lysosomes was reported in both MCF7 and PC3 cells, with highest correlation between 5-ALA and mitochondria in MCF7 cells [27]. Future work is required to dissect the spatio-temporal behaviour of 5-ALA signal distribution and its recruitment and localisation to the autophagy pathway intermediates. This may also include 5-ALA colocalisation to mitophagy events.

Our CLEM analysis confirmed 5-ALA fluorescence localisation largely to the autolysosomal and lysosomal compartment, which appear as distinctively electron-dense vesicle-like structures (Fig. 4). The localisation of 5-ALA in GBM cells to lysosomes and autolysosomes is, to our knowledge novel, and points to this specific pathway being engaged. We furthermore report that 5-ALA is found in electron-dense lysosomes and that 5-ALA-positive autophagosomes are markedly more electron dense, containing membrane-like cargo (Fig. 4 (ii, iii)). How 5-ALA is directed or recruited to autophagosomes, autolysosomes and lysosomes, remains unclear and requires further investigation. Our CLEM 2-D analysis of U118MG cells did not show well-defined, distinguishable mitochondria (Fig. 3). Instead, we observed large vacuole-like structures throughout the cytoplasm along with large lysosomes and autolysosomes (Fig. 3 (i-iv), Fig. S2 (i-iii)). This may reflect the typical phenotype of glioma cells with heightened autophagy activity and already dysfunctional mitochondria [28–30]. Due to the role of the haem biosynthetic pathway in 5-ALA metabolism, we investigated the localisation of 5-ALA to mitochondria. Indeed, although we observed a high portion of spatial colocalisation between these structures, taken together with the low Pearson's correlation coefficient, this may indicate a mere moderate correlation of 5-ALA with mitochondria (Fig. 1 G, H). Collectively, this data suggests a weaker interaction of 5-ALA signal with the mitochondrial network. This is possibly indicative of 5-ALA-positive material that has not yet dissociated from the mitochondria to be subsequently engulfed by autophagy intermediates. However, our results support the notion that both the autophagy machinery and mitochondria are related to 5-ALA derived fluorescence generation and that their dysfunction, as a component of the specific cancer pathology, may facilitate its preferential accumulation in GBM cells.

4.2. 5-ALA signal corresponds to areas of high autophagy flux

To better understand the relationship between autophagy activity and 5-ALA signal generation, we took advantage of a GFP LC3/RFP LC3 Δ G autophagy flux probe, allowing to observe cells with various degrees of autophagy activity across a single sphere. Our results revealed areas of increased autophagy flux, or 'flux hotspots' within the sphere (Fig. 2) where the ratio of GFP LC3/RFP LC3 Δ G was low corresponding to more RFP LC3 Δ G signal relative to GFP LC3 signal [24]. Intriguingly, 5-ALA signal appeared to be more intense at these flux hotspots, particularly after 24-h 5-ALA exposure (Fig. 2C, E), suggesting that increased autophagy activity, likely due to an increased number of autophagy pathway intermediates, corresponds to increased 5-ALA signal intensity. To our knowledge, this marks the first investigation to directly associate 5-ALA signal generation with autophagy activity, supporting the notion of autophagy control in the context of 5-ALA signal enhancement and thus providing mechanistic insights.

4.3. 3-D spheroid model system shows evidence for 5-ALA-induced mitophagy

The effect of 5-ALA exposure on the ultrastructural organisation in

GBM has remained largely unclear, especially in a spheroid model system. Therefore, Serial Block-Face Scanning Electron Microscopy (SBF-SEM) was performed, to characterise the spheroid in its entirety and to investigate the effects of 5-ALA exposure on cellular and subcellular organisation and integrity.

Our SBF analysis of U118MG spheres under control conditions revealed a distinct outer layer of loosely arranged cells (Fig. 5 A) which may correspond to the previously described proliferating zone [19]. The outermost border of 3-D spheroids has been suggested to be characteristic of the highly proliferative tumour margin that is typically in close proximity to capillaries [19]. To our surprise, these regions were significantly less prominent in the spheroids exposed to 5-ALA (Fig. 5 B), indicating potential effects of 5-ALA on the overall spheroid structural integrity. Upon further assessment at higher magnification and comparison of the mitochondrial network, a combination of fused and round, fragmented mitochondria with disrupted cristae were observed in control conditions (Fig. 5C). In sharp contrast, the mitochondrial network in 5-ALA treated spheroids was severely disrupted, indicating mitochondrial damage (Fig. 5 D). This 5-ALA-induced damage has been documented in monolayer model systems, however, not in a 3-D model [6,31–33].

Mitophagy has been described as the selective autophagic elimination of excess or damaged mitochondria [27,29,34]. Mitochondrial fragmentation and depolarisation are indeed prerequisites for the induction of mitophagy [29]. Our results reveal severe disruption of the internal organisation of mitochondrial morphology upon 5-ALA treatment, here the cristae are irregularly arranged with a disintegrated outer mitochondrial membrane (Fig. 5 D). Typically, cristae are well-defined extensions of the inner mitochondrial membrane, however GBM mitochondria have been described as abnormal with features of swelling and extensive cristolysis, i.e. the degradation of cristae, and an electron-lucent matrix [30]. One of the most intriguing observations in the 5-ALA treated spheres was the evidence for substantial mitophagy induction (Fig. 5 D). Here, we observed large, highly convoluted interconnected networks of double membranes engulfing distinctly circular mitochondria in response to 5-ALA exposure (Fig. 5). This response suggests robust induction of mitophagy where whole electron-lucent mitochondria are engulfed in double membranes [29,30]. Upon 5-ALA exposure, a multitude of round mitochondria, many of them having undergone complete cristolysis, were observed (Fig. 5 D). It is unclear whether the double membrane networks were derived from ER, Golgi or plasma membrane, since these have all been suggested to contribute to providing membrane material for autophagy [29]. We further assessed the effects of 5-ALA on spheroid integrity by volumetrically rendering the regions low in electron density in the spheroid core. Here, we observed a marked increase in the number and volume of such regions in the core of treated GBM spheroids (Fig. 5 E, F) – indicating a role of 5-ALA in compromising overall structural integrity. These observations support the notion of a potentially beneficial effect of 5-ALA exposure that could point towards additional treatment benefits when using 5-ALA, especially since a major challenge to cancer therapy is the ability to achieve drug penetration to particularly the core of the tumour, contributing to drug and radiation resistance [19].

A further characteristic of cancers is a hypoxic and necrotic core that is severely metabolite-deprived [19]. The characteristic features of necrosis include swelling of regions in the cytoplasm and cytoplasmic organelles, along with chromatin condensation [35]. We observed such characteristics for necrosis in control spheres (Fig. S3 (ii)) and more so identified necrotic cells towards the core region of 5-ALA treated spheroids (Fig. S3 (iv)).

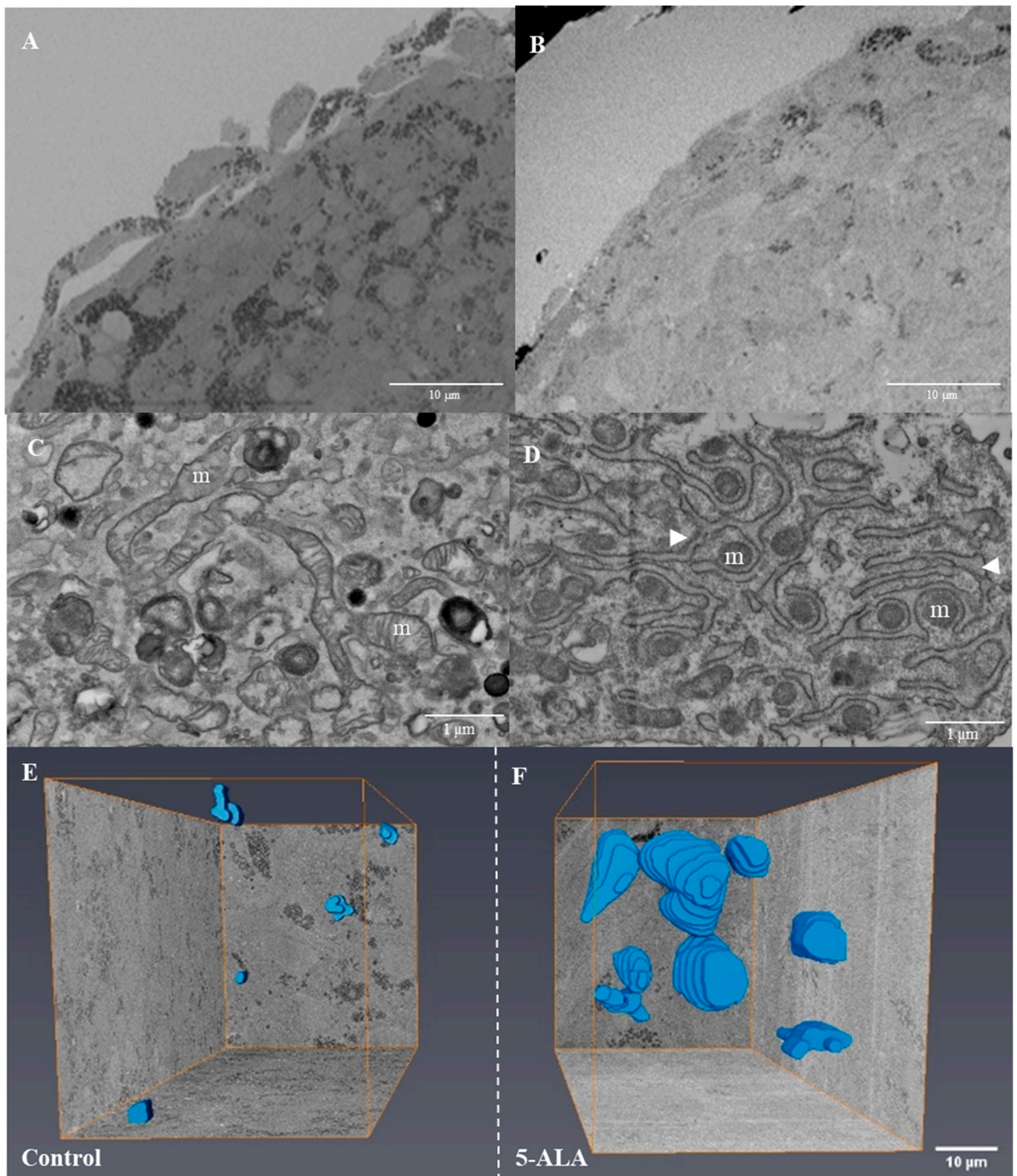


Fig. 5. A) The outer proliferating layer of untreated control spheroids are indicated with white arrowheads alongside higher resolution micrographs of treated spheroids (B). C) EM micrographs showing ultrastructural detail of cytoplasmic, well-defined mitochondrial network in control U118MG spheroids. D) EM micrographs showing mitochondrial network and altered morphology towards a fragmented ultrastructural phenotype in U118MG spheroids treated for 6 h with 5 mM 5-ALA. E) Volumetric rendering of regions low in electron density in control U118MG spheroids. F) Volumetric rendering of regions low in electron density, in U118MG spheroids treated with 5 mM 5-ALA for 6 h. Scale bar: 1 μm and 100 μm .

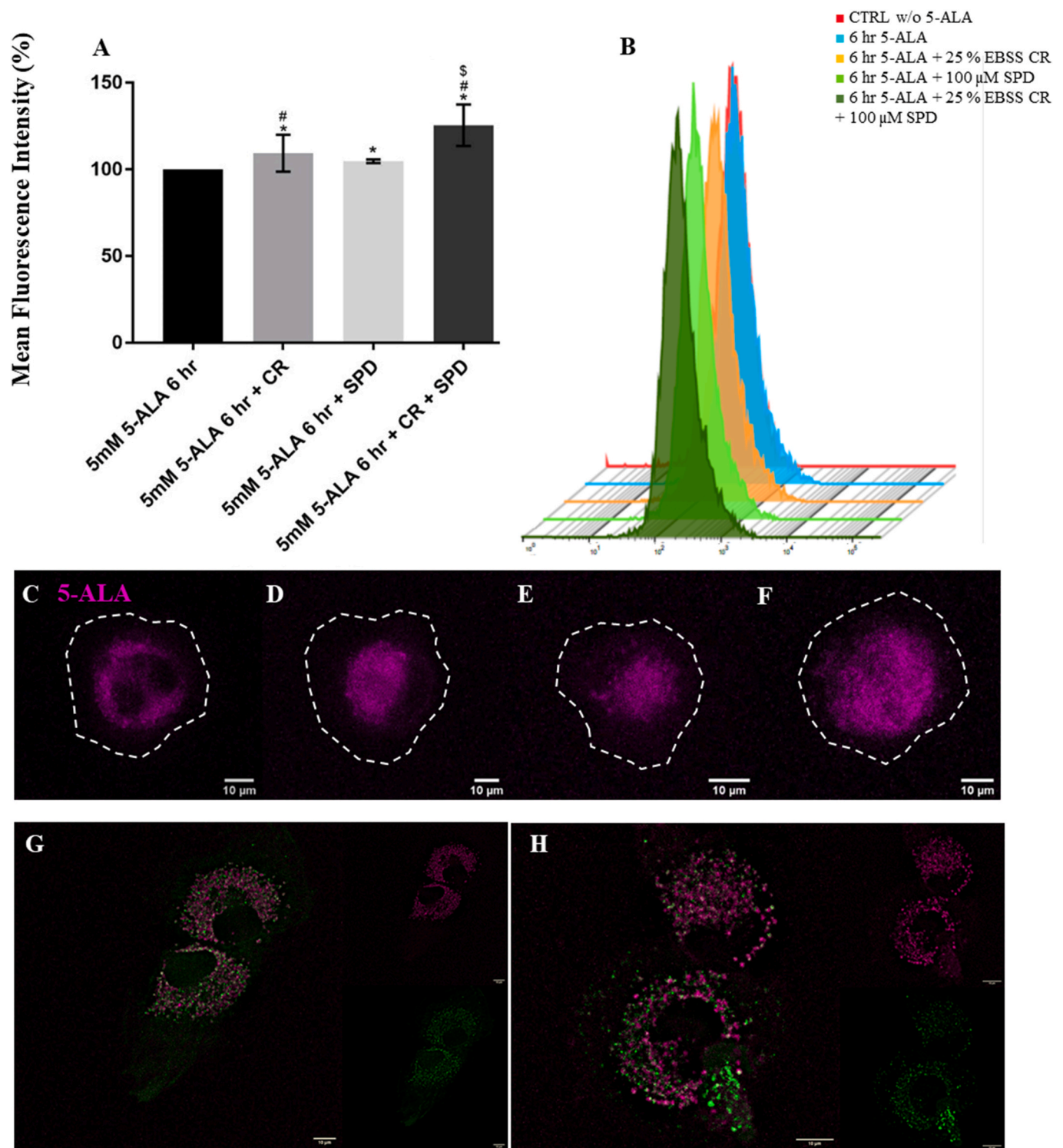


Fig. 6. Flow cytometry-based mean fluorescence intensity analysis following 6 h 5 mM 5-ALA treatment of U118MG cells in combination with autophagy-induction. A) U118MG cells were treated with 5 mM 5-ALA in combination with 3 h 25 % EBSS CR (Caloric Restriction), 24-h 100 μ M SPD (Spermidine) and a combination treatment of 24-h 100 μ M SPD and 3-h CR exposure. * $p < 0.05$ vs. 5 mM 5-ALA, # $p < 0.05$ vs. 5 mM 5-ALA +100 μ M SPD, \$ $p < 0.05$ vs. 5 mM 5-ALA +100 μ M SPD +25 % EBSS CR. N = 3, 15 000 events acquired per N. B) Representative intensity histogram showing mean fluorescence intensity of all treatment groups and untreated control cells. C) Fluorescence micrographs showing U118MG cells treated with 5 mM 5-ALA for 6 h, D) U118MG cells treated with a combination of 5 mM 5-ALA for 6 h and 25 % EBSS for 3 h, E) U118MG cells treated with a combination of 100 μ M SPD for 24 h and 5 mM 5-ALA for 6 h, F) U118MG cells treated with a combination of 100 μ M SPD for 24 h, 5 mM 5-ALA for 6 h and 25 % EBSS for 3 h. G) GFP-LC3-transfected U118MG cells treated with 5 mM 5-ALA for 6 h followed by exposure to 400 nM Bafilomycin A1 for 4 h. FM images acquired using 63 \times magnification, scale bar: 10 μ m.

4.4. Autophagy enhancement increases 5-ALA signal intensity

It is clear at this point that autophagic pathway intermediates are associated with 5-ALA signal localisation; however, whether autophagy enhancement may impact signal intensity is not known. Hence, this relationship was further explored through flow cytometry analysis in response to autophagy enhancement, using Spermidine (SPD) [36] and caloric restriction (CR) intervention [37]. Indeed, a significant increase in 5-ALA derived fluorescence intensity was observed in response to SPD, CR and combination SPD/CR treatment (Fig. 6 A). Here, the lowest relative increase in 5-ALA signal intensity was observed in response to SPD treatment, with CR showing a slightly greater increase relative to the highest fluorescence intensity observed in response to the CR and SPD combination treatment (Fig. 6 A, C–F).

As far as we know, the 5-ALA signal intensity-enhancing effects of autophagy induction using Spermidine and CR have not previously been shown and provide insights into the mechanisms governing 5-ALA fluorescence in GBMs. Importantly, this observation could potentially inform the future development of new workflows for 5-ALA FGR that incorporates fasting (CR) or SPD treatment prior to 5-ALA administration given that SPD is available as an over-the-counter supplement and could therefore be rapidly implemented in the clinical setting [37,38]. Caloric restriction is currently being investigated in its effectiveness in enhancing cancer immunosurveillance and thereby sensitising cells to chemotherapy-induced death. These studies are largely based on *in vitro*-based experimental findings where CR effectively inhibits tumour growth [37,39]. It is likely that increased autophagy activity could, through promoting the clearance of dysfunctional mitochondria, improve activity in healthy mitochondria, consequently promoting 5-ALA metabolism and increasing signal intensity [40,41]. This hypothesis deserves further investigation.

Taken together, this data suggests that indeed autophagy modulation, through gross signal intensity enhancement, could facilitate increased 5-ALA signal intensity in poorly fluorescing tumour tissue areas, i.e. peripheral regions [9]. In doing so, the low infiltrative tumour tissue at the periphery of GBM that usually shows no visible fluorescence with the conventional technique might be better identified in the future. Furthermore, the described increased 5-ALA signal intensity might be able to visualize the usually non-detectable tumour tissue of low-grade gliomas during surgery as well. This will result in a distinct increase of the extent of resection during surgery of both high- and low-grade gliomas and thus patient prognosis. Furthermore, the efficiency of photodynamic therapy of recurrent GBM might be dramatically improved by this approach. In addition, the inclusion of SPD and CR regimen into GBM management may play a favourable role in reactivating immunosurveillance and thereby enhancing sensitivity of GBM cells to the secondary photochemically-induced oxidative stress and subsequent cell death induction [2,42]. Taken together, it becomes clear that autophagy control may serve as an attractive avenue for improving future interventions aimed towards maximizing safe resection of GBMs and with that an improved prognosis.

5. Summary and conclusion

The here presented 5-ALA fluorescence signal localisation predominantly to lysosomes and autolysosomes may provide novel insights into 5-ALA-associated metabolism and the mechanisms involved in fluorescence signal generation. The key implications include that firstly, the signal-enhancing effects through autophagy induction suggest that indeed the autophagy pathway intermediates play a critical role in 5-ALA fluorescence metabolism and signal generation. Secondly, the observed mitophagy engagement together with cytoplasmic vacuolisation in response to 5-ALA exposure points to an additional mechanism of 5-ALA, contributing to a highly disruptive cellular phenotype, possibly contributing to cell death sensitisation. Thirdly, 5-ALA-treated spheroids showed more compact proliferative borders, indicating a potentially

beneficial effect of 5-ALA administration in condensing the proliferative tumour margins of glioma cells. Finally, and may be most importantly, 5-ALA-derived signal enhancement through autophagy induction using CR and SPD exposure, as employed in this study, may serve as a point of departure for clinical implementation to improve EoR and further surgical approaches in the management of GBM. Considering the many metabolic perturbations that accompany glioblastomas, autophagy modulation serves as a promising target for improved therapy [43]. A major need remains to characterise, in more depth, 5-ALA-related signal dynamics and their potential to facilitate greater EoR, ultimately towards maximal safe surgical resection to improve patient prognosis and to offset GBM recurrence. The significant increase in 5-ALA signal intensity due to autophagy upregulation lends itself to further incorporating emerging autophagy-enhancing drugs such as resveratrol or metformin (Coyle et al., 2016; Ko et al., 2017; Sahra et al., 2010) to further assess and improve the efficacy of such surgical interventions.

Ethical approval

Not applicable.

Funding

We wish to acknowledge financial support from the Cancer Association South Africa (CANSA) and thank the Central Analytical Facility, Stellenbosch University, for the use of the instruments.

Availability of data and materials

Not applicable.

CRediT authorship contribution statement

Kim Fredericks: Writing – original draft, Investigation, Formal analysis. **Jurgen Kriel:** Writing – review & editing, Visualization, Methodology. **Lize Engelbrecht:** Writing – review & editing, Visualization, Methodology. **Petra Andreea Mercea:** Writing – review & editing, Validation, Resources, Conceptualization. **Georg Widhalm:** Writing – review & editing, Validation, Resources, Conceptualization. **Brad Harrington:** Writing – review & editing, Validation, Resources, Conceptualization. **Ian Vlok:** Writing – review & editing, Validation, Methodology, Conceptualization. **Ben Loos:** Writing – review & editing, Resources, Funding acquisition, Conceptualization.

Declaration of competing interest

I wish to confirm that no conflict of interest exists. The manuscript has not been submitted for publication elsewhere.

Data availability

Data will be made available on request.

Appendix A. Supplementary data

Supplementary data to this article can be found online at <https://doi.org/10.1016/j.bbrep.2024.101642>.

References

- [1] R. Stupp, W.P. Mason, M.J. van den Bent, M. Weller, B. Fisher, M.J.B. Taphoorn, K. Belanger, A.A. Brandes, C. Marosi, U. Bogdahn, J. Curschmann, R.C. Janzer, S. K. Ludwin, T. Gorlia, A. Allgeier, D. Lacombe, J.G. Cairncross, E. Eisenhauer, R. O. Mirimanoff, Radiotherapy Plus Concomitant and Adjuvant Temozolomide for Glioblastoma, vol. 352, 2009, pp. 987–996, <https://doi.org/10.1056/nejmoa043330>, 10.

- [2] C. Dupont, N. Betrouni, S.R. Mordon, N. Reyns, M. Vermandel, 5-ALA photodynamic therapy in neurosurgery, towards the design of a treatment planning system: a proof of concept, *IRBM* 38 (1) (2017) 34–41.
- [3] W. Stummer, Extent of resection and survival in glioblastoma Multiforme: identification of and adjustment for bias, *Clin. Res.* 62 (3) (2008) 564–576.
- [4] L. Wei, Y. Fujita, N. Sanai, J.T.C. Liu, Toward quantitative neurosurgical guidance with high-resolution microscopy of 5-aminolevulinic acid-induced protoporphyrin IX, *Front. Oncol.* 9 (2019) 592.
- [5] S. Zhao, J. Wu, C. Wang, H. Liu, X. Dong, C. Shi, C. Shi, Y. Liu, L. Teng, D. Han, X. Chen, G. Yang, L. Wang, C. Shen, H. Li, Intraoperative fluorescence-guided resection of high-grade malignant gliomas using 5-aminolevulinic acid-induced porphyrins: a systematic review and meta-analysis of prospective studies, *PLoS One* 8 (5) (2013) e63682.
- [6] S.L. Gibbs, B. Chen, J.A. O'Hara, P.J. Hoopes, T. Hasan, B.W. Pogue, Protoporphyrin IX level correlates with number of mitochondria, but increase in production correlates with tumor cell size, *Photochem. Photobiol.* 82 (5) (2006) 1334.
- [7] H. Stepp, W. Stummer, 5-ALA in the management of malignant glioma, *Laser Surg. Med.* 50 (5) (2018) 399–419.
- [8] W. Stummer, U. Pichlmeier, T. Meinel, O.D. Wiestler, F. Zanella, H.J. Reulen, Fluorescence-guided surgery with 5-aminolevulinic acid for resection of malignant glioma: a randomised controlled multicentre phase III trial, *Lancet Oncol.* 7 (5) (2006) 392–401.
- [9] M.J. Colditz, K. van Leyen, R.L. Jeffree, Aminolevulinic acid (ALA)–protoporphyrin IX fluorescence guided tumour resection. Part 2: theoretical, biochemical and practical aspects, *J. Clin. Neurosci.* 19 (12) (2012) 1611–1616.
- [10] E. Rampazzo, A. della Puppa, C. Frasson, G. Battilana, S. Bianco, R. Scienza, G. Basso, L. Persano, Phenotypic and functional characterization of Glioblastoma cancer stem cells identified through 5-aminolevulinic acid-assisted surgery, *J. Neuro-Oncol.* 116 (3) (2014) 505–513.
- [11] A. v Onorati, M. Dyczynski, R. Ojha, R.K. Amaravadi, Targeting autophagy in cancer, *Cancer* 124 (2018) 3307–3318.
- [12] A.M. Cuervo, Autophagy: in sickness and in health, *Trends Cell Biol.* 14 (2) (2004) 70–77.
- [13] J. Kriegl, B. Loos, The good, the bad and the autophagosome: exploring unanswered questions of autophagy-dependent cell death, *Cell Death Differ.* 26 (4) (2019) 640–652.
- [14] E. Pawlowska, J. Szczepanska, M. Szatkowska, J. Blasiak, An interplay between senescence, apoptosis and autophagy in glioblastoma multiforme—role in pathogenesis and therapeutic perspective, *Int. J. Mol. Sci.* 19 (3) (2018) 889.
- [15] K.M. Ryan, P53 and autophagy in cancer: guardian of the genome meets guardian of the proteome, *Eur. J. Cancer* 47 (1) (2011) 44–50.
- [16] V. Herceg, N. Lange, E. Allemann, A. Babic, Activity of phosphatase-sensitive 5-aminolevulinic acid prodrugs in cancer cell lines, *J. Photochem. Photobiol. B Biol.* 171 (2017) 34–42.
- [17] P.S. Jones, A. Yekula, E. Lansbury, J.L. Small, C. Ayinon, S. Mordecia, F. H. Hochberg, J. Tigges, B. Delcuze, A. Charest, I. Ghiran, L. Balaj, B.S. Carter, Characterization of plasma-derived protoporphyrin-IX-positive extracellular vesicles following 5-ALA use in patients with malignant glioma, *EBioMedicine* 48 (2019) 23–35.
- [18] Y. Kitajima, T. Ishii, T. Kohda, M. Ishizuka, K. Yamazaki, Y. Nishimura, T. Tanaka, S. Dan, M. Nakajima, Mechanistic study of PpIX accumulation using the JFCR39 cell panel revealed a role for dynamin 2-mediated exocytosis, *Sci. Rep.* 9 (1) (2019) 8666.
- [19] M.J. Ware, K. Colbert, V. Keshishian, J. Ho, S.J. Corr, S.A. Curley, B. Godin, Generation of homogenous three-dimensional pancreatic cancer cell spheroids using an improved hanging drop technique, *Tissue Eng. C Methods* 22 (4) (2016) 312–321.
- [20] S. de Wet, A. Du Toit, B. Loos, Spermidine and rapamycin reveal distinct autophagy flux response and cargo receptor clearance profile, *Cells* 10 (1) (2021) 95.
- [21] J. Kriegl, K. Müller-Nedebock, G. Maarman, S. Mbizana, E. Ojuka, B. Klumperman, B. Loos, Coordinated autophagy modulation overcomes glioblastoma chemoresistance through disruption of mitochondrial bioenergetics, *Sci. Rep.* 8 (1) (2018) 10348.
- [22] F. Soulez, L. Denis, Y. Tourneur, E. Thiébaud, Blind deconvolution of 3D data in wide field fluorescence microscopy, in: International Symposium on Biomedical Imaging, CDROM, Barcelona, Spain, May 2012 ffnal-00691249.
- [23] P. Schober, L.A. Schwarte, Correlation coefficients: appropriate use and interpretation, *Anesth. Analg.* 126 (5) (2018) 1763–1768.
- [24] T. Kaizuka, H. Morishita, Y. Hama, S. Tsukamoto, T. Matsui, Y. Toyota, A. Kodama, T. Ishihara, T. Mizushima, N. Mizushima, An autophagic flux probe that releases an internal control, *Mol. Cell* 64 (4) (2016) 835–849.
- [25] C.J. Peddie, K. Blight, E. Wilson, C. Melia, J. Marrison, R. Carzaniga, M.-C. Domart, P. O'Toole, B. Larijani, L.M. Collinson, Correlative and integrated light and electron microscopy of in-resin GFP fluorescence, used to localise diacylglycerol in mammalian cells, *Ultramicroscopy* 143 (100) (2014) 3.
- [26] P. Paul-Gilloteaux, X. Heiligenstein, M. Belle, M.-C. Domart, B. Larijani, L. Collinson, G. Raposo, J. Salamero, eC-CLEM: flexible multidimensional registration software for correlative microscopies, *Nat. Methods* 14 (2) (2017) 102–103.
- [27] M. Sasaki, M. Tanaka, H. Ichikawa, T. Suzuki, H. Nishie, K. Ozeki, T. Shimura, E. Kubota, S. Tanida, H. Kataoka, 5-aminolevulinic acid (5-ALA) accumulates in GIST-T1 cells and photodynamic diagnosis using 5-ALA identifies gastrointestinal stromal tumors (GISTs) in xenograft tumor models, *PLoS One* 16 (4) (2021) e0249650.
- [28] H. Maes, N. Rubio, A.D. Garg, P. Agostinis, Autophagy: shaping the tumor microenvironment and therapeutic response, *Trends Mol. Med.* 19 (7) (2013) 428–446.
- [29] A.S. Rambold, J. Lippincott-Schwartz, Mechanisms of mitochondria and autophagy crosstalk, *Cell Cycle* 10 (23) (2011) 4032–4038.
- [30] T.N. Seyfried, R.E. Flores, A.M. Poff, D.P. D'Agostino, Cancer as a metabolic disease: implications for novel therapeutics, *Carcinogenesis* 35 (3) (2014) 515–527.
- [31] M. Hermes-Lima, V.G.R. Valle, A.E. Vercesi, E.J.H. Bechara, Damage to rat liver mitochondria promoted by δ -aminolevulinic acid-generated reactive oxygen species: connections with acute intermittent porphyria and lead-poisoning, *Biochim. Biophys. Acta Bioenerg.* 1056 (1) (1991) 57–63.
- [32] J. Onuki, Y. Chen, P.C. Teixeira, R.I. Schumacher, M.H.G. Medeiros, B. van Houten, P. di Mascio, Mitochondrial and nuclear DNA damage induced by 5-aminolevulinic acid, *Arch. Biochem. Biophys.* 432 (2004) 178–187.
- [33] J. Zhu, K.Z. Wang, C.T. Chu, After the banquet, *Autophagy* 9 (11) (2013) 1663–1676.
- [34] L.C. Gomes, G. di Benedetto, L. Scorrano, During autophagy mitochondria elongate, are spared from degradation and sustain cell viability, *Nat. Cell Biol.* 13 (5) (2011) 589–598.
- [35] L. Galluzzi, M.C. Maiuri, I. Vitale, H. Zischka, M. Castedo, L. Zitvogel, G. Kroemer, Cell death modalities: classification and pathophysiological implications, *Cell Death Differ.* 14 (7) (2007) 1237–1243.
- [36] F. Madeo, T. Eisenberg, S. Büttner, C. Ruckenstein, G. Kroemer, Spermidine: a novel autophagy inducer and longevity elixir, *Autophagy* 6 (1) (2010) 160–162.
- [37] F. Pietrocola, J. Pol, E. Vacchelli, S. Rao, D.P. Enot, E.E. Baracco, S. Levesque, F. Castoldi, N. Jacquilot, T. Yamazaki, L. Senovilla, G. Marino, F. Aranda, S. Durand, V. Sica, A. Chery, S. Lachkar, V. Sigl, N. Bloy, A. Buque, S. Falzoni, B. Ryffel, F. di Virgilio, F. Madeo, M.C. Maiuri, L. Zitvogel, B. Levine, J. M. Penninger, G. Kroemer, Caloric restriction mimetics enhance anticancer immunosurveillance, *Cancer Cell* 30 (1) (2016) 147–160.
- [38] F. Madeo, M.A. Bauer, D. Carmona-Gutierrez, G. Kroemer, Spermidine: a physiological autophagy inducer acting as an anti-aging vitamin in humans? *Autophagy* 15 (1) (2019) 165–168.
- [39] S. Lévesque, J.G. Pol, G. Ferrere, L. Galluzzi, L. Zitvogel, G. Kroemer, Trial watch: dietary interventions for cancer therapy, *OncolImmunology* 8 (7) (2019) 1–8.
- [40] A.M. Cuervo, E. Bergamini, U.T. Brunk, W. Dröge, M. Ffrench, A. Terman, Autophagy and aging: the importance of maintaining “clean” cells, *Autophagy* 1 (3) (2005) 131–140.
- [41] K. Palikaras, E. Lionaki, N. Tavernarakis, Balancing mitochondrial biogenesis and mitophagy to maintain energy metabolism homeostasis, *Cell Death Differ.* 22 (2015) 1399–1401.
- [42] M. Wachowska, A. Muchowicz, M. Firczuk, M. Gabrysiak, M. Winiarska, M. Wańczyk, K. Bojarczuk, J. Golab, Aminolevulinic acid (ALA) as a prodrug in photodynamic therapy of cancer, *Molecules* 16 (5) (2011) 4140–4164.
- [43] R. Rangwala, R. Leone, Y.C. Chang, L.A. Fecher, L.M. Schuchter, A. Kramer, K. S. Tan, D.F. Heitjan, G. Rodgers, M. Gallagher, S. Piao, A.B. Troxel, T.L. Evans, A. M. DeMichele, K.L. Nathanson, P.J. O'Dwyer, J. Kaiser, L. Pontiggia, L.E. Davis, R. K. Amaravadi, Phase I trial of hydroxychloroquine with dose-intense temozolomide in patients with advanced solid tumors and melanoma, *Autophagy* 10 (8) (2014) 1369–1379.